Polymer Bulletin
https://doi.org/10.1007/s00289-024-05226-9

ORIGINAL PAPER

Synthesis and characterization of ureidopyrimidinone-functionalized polyurethane acrylates and their hybrid nanocomposites for UV coating applications

Mert Çınar[1] · Gökhan Çaylı[2] · Sevim Karataş[1]

Received: 29 November 2023 / Revised: 4 February 2024 / Accepted: 23 February 2024
© The Author(s) 2024

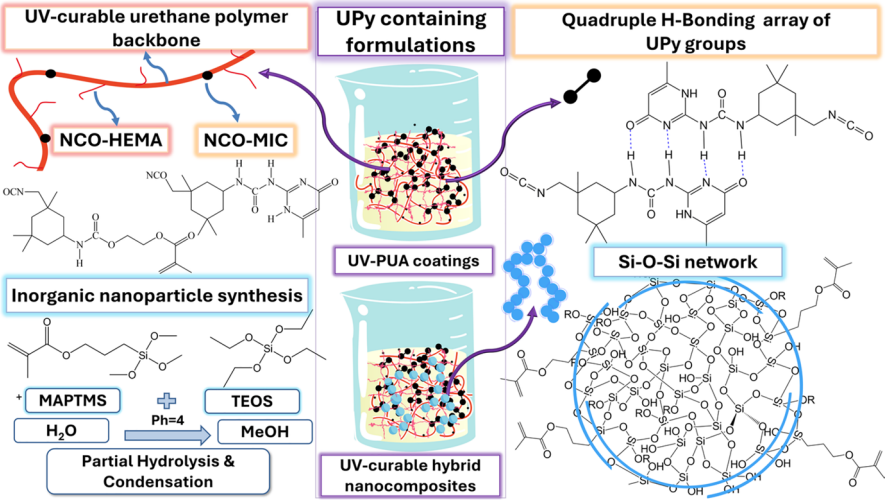
Abstract

In this study, ureidopyrimidinone moieties (UPy), capable of physical crosslinking via quadruple hydrogen bonding, were successfully incorporated into UV-curable polyurethane acrylate prepolymers. First, a hydroxyl-terminated unsaturated ester monomer was synthesized and reacted with isophorone diisocyanate to create a hydroxyl-terminated UV-curable urethane oligomer (U–OH). Then, isocyanate-terminated building blocks (UPy moieties and an acrylate-based photosensitive monomer) were synthesized and used in various ratios to functionalize U–OH for the preparation of a series of UV-curable UPy-containing polyurethane acrylate (PUA) resins. The resulting products were structurally characterized using ^{1}H NMR and FTIR spectroscopy. Furthermore, organic–inorganic hybrid nanocomposites were obtained by introducing silane coupling agents into PUA resins using the sol–gel process. A series of UV-curable UPy-containing PUA coatings and hybrid nanocomposites were prepared, and their synergistic effect on coating properties was investigated. The dynamic mechanical analysis revealed that the Tg of the samples increased with increasing UPy content, although the mechanical properties remained largely unaltered, as shown by the stress–strain test. The studies also demonstrated that the hybrid nanocomposites exhibited higher decomposition temperatures and better thermal stability compared to pure PUAs. All the coatings exhibited good transparency in the visible region. An optical microscope was used to investigate the self-healing property by scratching the plexiglass panels with a razor blade. Among the other samples, the coating with the highest percentage of UPy content exhibited the best self-healing ability after heat treatment at 90 °C for 10 min.

Extended author information available on the last page of the article

Published online: 25 March 2024

Graphical abstract



Keywords Ureidopyrimidinone · UV-curable · Polyurethane acrylate · Coating · Self-healing · Nanocomposites

Introduction

UV-curable materials are widely used for many applications due to their economic and environmental aspects, as well as their energy-saving and fast-curing properties [1, 2]. Polyurethane acrylates (PUAs) are an important class of UV-curable polymers that are frequently used as protective coatings because of their adaptability through composition modification. Moreover, they exhibit excellent resistance to chemicals, abrasion, and temperature, making them ideal for indoor applications [3–5]. However, when used outdoors, PUAs tend to degrade under environmental stress such as heat, moisture, and radiation. Therefore, improvement of PUAs' thermal and mechanical properties is crucial, and many research groups focus on this issue [6–8].

One promising strategy to enhance PUAs' thermal and mechanical properties is functionalization with supramolecular moieties [9, 10]. In nature, biological functions rely on non-covalent interactions, as observed in DNA pairing where the hydrogen bonding plays a key role between complementary base pairs such as adenine and thymine that are held together by two hydrogen bonds, which is essential for replication and transcription of genetic information [11, 12]. However, the limited number of hydrogen bonds in supramolecular groups is not enough to achieve desired properties, and thus it would be necessary to use materials that can form multiple hydrogen bonds and apply them in polymeric materials. Taking its inspiration from nature, in 1997, Meijer and coworkers [13] reported quadrupole

H-bonding arrays with a high degree of dimerization constant (K_{dim} of 6×107 M^{-1} in $CHCl_3$) named 2-ureido-4[1H]-pyrimidinone group (UPy), which have gained considerable attention since then [14, 15]. Their ability to form self-complimentary UPy dimers leads to physical crosslinking, which has allowed for the development of materials with enhanced mechanical, optical, and biomedical properties [16–18]. The incorporation of multiple hydrogen-bonding units that are sensitive to changes in temperature, pH, or other environmental conditions can be used to create stimuli-responsive polymers. These polymers can be used as sensors or actuators. Hence, with the aid of these properties, it is possible to develop polymers with unique properties such as self-healing, shape memory effect, reversible crosslinking, and multi-responsiveness [19–22].

Drawing on this concept, Invernizzi and coworkers [23] prepared a novel 4D printable shape memory polymer with self-healing ability at 80 °C by combining UV-curable polycaprolactone dimethyl acrylate (PCLDMA) macromonomers with UPy-bearing MMA adduct (UPyMA), which was synthesized by the reaction between 6-methylisocytosine (6-MIC) and 2-isocyanatoethyl methacrylate (2-IEM). In the printable formulation, the weight percentage of UPyMA was kept between 2 and 5 wt% with respect to the weight of PCLDMA and UPyMA, and the mixture was combined with 4 wt% of photoinitiator and 60 wt% $CHCl_3$. They found that the mechanical properties of the printed and PCDL-based cast samples were similar. Printed and repaired materials showed good healing efficiency and could be used as actuator devices in soft robotics applications.

Gao et al. [24] prepared a series of UV-curable PU oligomers by functionalizing polycarbonate diols (PCDL) with UPy groups (PCDL-PU-UPy) and used different types and amounts of reactive diluents to study their effect on coatings properties. The coatings showed good thermal stability and adhesion and exhibited self-healing ability at 70 °C. They also found that with the increasing functionality of the reactive diluent, a more complex 3D network was achieved, which prevented polymer chains from moving freely and hindered the diffusion of species in the crack, resulting in a decrease in self-healing ability.

Another way to enhance the coating performance of UV-curable materials is to increase crosslinking density by introducing silane coupling agents into the polymer matrix through the sol–gel process [25, 26]. This method involves the combination of inorganic and organic units at the molecular and nanoscale levels through covalent bonds and overcomes the thermodynamically poor affinity of these materials [27, 28]. The silane precursors form a strong Si–O–Si network by undergoing hydrolysis and condensation reactions under mild conditions in the presence of acid or base catalyst. By the dispersion of the prehydrolyzed inorganic sol into polymer coatings, organic–inorganic (O–I) hybrid nanocomposite materials are produced. This easy method is often used in manufacturing clear coats and optical coatings [29, 30].

The use of ureidopyrimidinone-functionalized polyurethane acrylates in UV-curable coatings has been limitedly studied. This study aims to synthesize and characterize UV-curable UPy-containing PUAs along with their O–I hybrid nanocomposites. For this purpose, two building blocks were synthesized to modify PUAs. An isocyanate-terminated methylisocytosine building block (NCO-MIC) was prepared

by reacting 6-MIC with isophorone diisocyanate (IPDI). The physical crosslinking ability of NCO-MIC groups was demonstrated through dimerization via quadruple H-bonding arrays to form UPy moieties. An acrylate-based building block (NCO-HEMA) was utilized as a photosensitive monomer. Subsequently, a UV-curable hydroxyl-terminated unsaturated ester (UnE–OH) monomer was synthesized and reacted with IPDI to obtain a UV-curable hydroxyl-terminated urethane oligomer (U–OH), which served as the main chain of all the polyurethanes. UV-curable PUA resins were formed by incorporating different contents of NCO-HEMA and NCO-MIC building blocks into U–OH. Hybrid nanocomposites of the PUAs were prepared using the sol–gel method. The resulting UV-cured coating materials were characterized by their mechanical, physical, morphological, and thermal properties.

Experimental

Materials and methods

2-Hydroxyethyl methacrylate (HEMA) and tetraethyl orthosilicate (TEOS) were supplied from Merck. Darocur 1173 (DR1173) from Ciba Specialty Chemicals Inc., was used as a photoinitiator; ρ-toluene sulfonic acid (PTSA) was purchased from Fluka. Itaconic Acid (IA), allyl glycidyl ether (AGE), methyl methacrylate (MMA), 2-amino-4-hydroxy-6-methylpyrimidine (6-MIC), [3-(methacryloyloxy)propyl] trimethoxysilane (MAPTMS), methanol, and chloroform ($CHCI_3$) were supplied from Sigma-Aldrich Inc., (Shanghai, China) and were used as received. Isophorone diisocyanate (IPDI; pure grade, 98%) was purchased from Alfa Aesar (Massachusetts, USA). Teflon TM templates (50 mm × 10 mm × 1 mm) were used to cast the free films. The UV lamp (UltraVitalux 300 W 230 V E27) was purchased from Osram. Plexiglass test panels (70 mm × 70 mm × 1 mm) were purchased from local suppliers.

Synthesis of isocyanate-functionalized methylisocytosine building block (NCO-MIC)

NCO-MIC (UPy moieties) was synthesized according to the literature [31]. The synthesis pathway is given in Fig. 1a. In a three-necked round-bottomed flask, 10.4 g of 6-MIC was dissolved in 40 ml of $CHCI_3$. Then 80 ml of IPDI was added dropwise under nitrogen atmosphere for 1 h. The system was equipped with a mechanical stirrer, a condenser, a dropping funnel, and a nitrogen inlet. The temperature of the reaction mixture was set to 90 °C. After vigorously stirring for three days, a clear solution was obtained. Then the solution was precipitated in 300 ml of heptane in an ice bath, resulting in a white gum, washed with heptane until a solid white powder was obtained. The yield of the reaction was 95.3%.

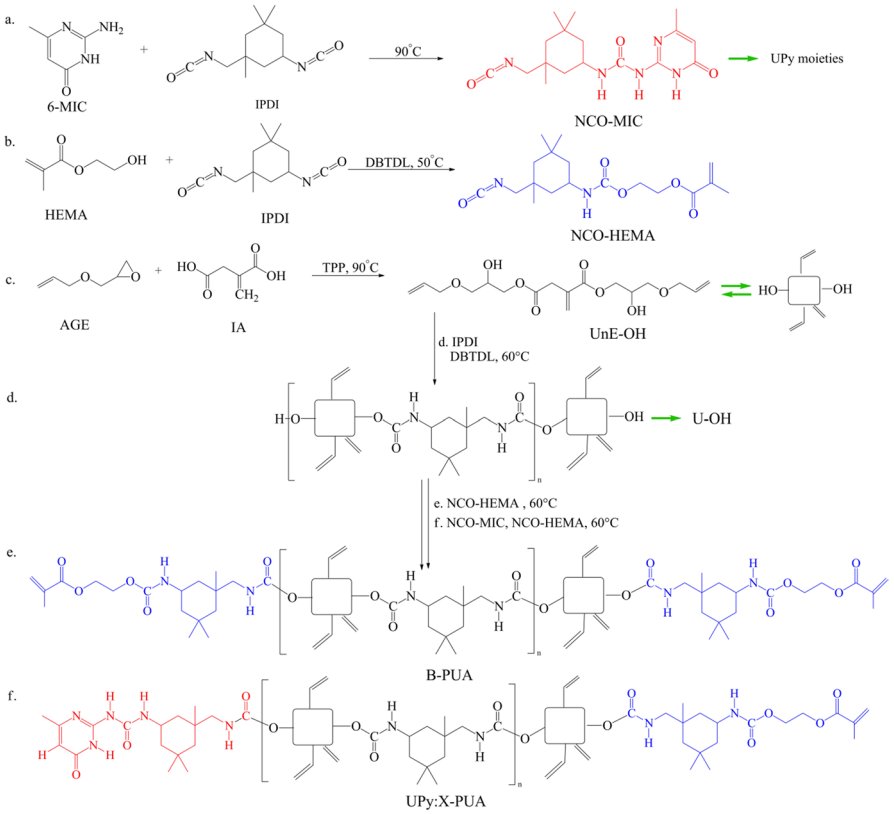


Fig. 1 Schematic route for the preparation of the UV-curable UPy-containing PUAs

^{1}H NMR (chloroform-*d*): δ 13.04 (s, 1H, CH_3–C–N**H**), 11.86 (s, 1H, CH_2–N**H**–(C=O)–NH), 10.00 (m, 1H, CH_2–NH–(C=O)–N**H**), 5.82 (s, 1H, C=C**H**–(C=O)), 4.1–3.2.5 (m, 3H, NH–C**H**–(CH_2)2, O=C=N–C**H$_2$**), 2.22 (s, 3H, NH–C(C**H$_3$**)=CH), 1.98–0.95 (m, 4H; m 15H, isophorone moieties).

Synthesis of acrylate-based building block (NCO-HEMA)

As depicted in Fig. 1b, NCO-HEMA, a photosensitive monomer, was synthesized to functionalize the urethane oligomer. Under nitrogen input, 11.115 g (0.05 mol) of IPDI was dissolved in $CHCl_3$. Then it was charged into a three-necked round-bottomed flask with DBTDL as a catalyst. After that, 6.0507 g (0.05 mol) of HEMA, dissolved in 20 ml of $CHCl_3$, was added dropwise into the flask. The reaction mixture was heated to 50 °C for 3 h. Finally, a clear acrylate-based building block was obtained.

Synthesis of hydroxyl-terminated unsaturated urethane oligomer (U–OH)

U–OH was used as a main chain in all PUAs polymer backbone and synthesized in two steps. The schematic route of the synthesis is shown in Fig. 1c and d. An unsaturated ester-based hydroxyl-terminated monomer (UnE-OH) was synthesized in the first step. In a three-necked round-bottomed flask equipped with a mechanical stirrer and condenser, 19.52 g (0.15 mol) of IA, 34.24 g (0.3 mol) of AGE, and 0.5 wt.% (0.26 g) of TPP as catalyst were mixed under nitrogen atmosphere. Then the mixture was heated to 90 °C. When a clear solution was formed, the temperature increased to 120 °C, and the reaction proceeded until all epoxy groups were consumed. In the second step, the reaction mixture was cooled down to 50 °C, and 22.23 g (0.1 mol) of IPDI and DBTDL were added to achieve a hydroxyl-terminated urethane oligomer. The synthesis was completed in 5 h, and a slightly yellow-colored clear U–OH oligomer was obtained.

Synthesis of UV-curable PUA and UPy-containing PUA resins

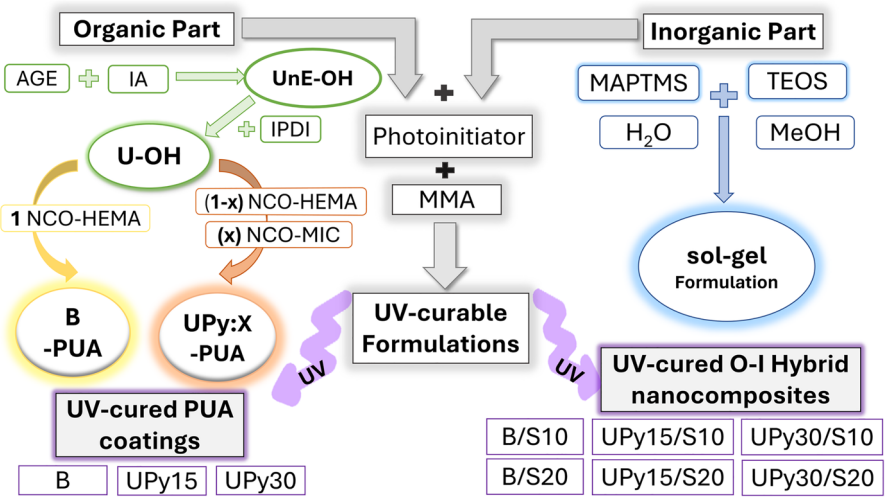
UV-curable PUA resins were synthesized by varying the quantities of NCO-HEMA and NCO-MIC. These resins are called as B-PUA and UPy:X-PUA (UPy:15-PUA and UPy:30-PUA), where X represents the %(w/w) molar ratio of UPy moieties in the isocyanate building block contents. The final products are represented in Fig. 1e–f. Neat resin (B-PUA) was synthesized by the reaction between U–OH and NCO-HEMA. The solids concentration of the reaction mixtures was adjusted to 80% w/v using $CHCI_3$. The compositions and molar ratios of the UV-curable PUA and UPy:X-PUA resins are listed in Table 1. A brief description of the synthesis of UPy-containing PUA is as follows: U–OH dissolved in $CHCI_3$ was added to a three-necked round-bottomed flask. The system was equipped with a mechanical stirrer, a condenser, a dropping funnel, and a nitrogen input. The reaction mixture was heated to 60 °C. Then, DBTDL as catalyst and required amount of suitable NCO building blocks that contains different proportions of NCO-HEMA and NCO-MIC in $CHCI_3$ were added dropwise to the reaction mixture, respectively. The reaction was continued until all NCO content was consumed.

Table 1 The composition of UV-curable PUA resins

PUA resins	U–OH oligomer		NCO-HEMA		NCO-MIC	
	(g)	(eq. mol)	(g)	(eq. mol)	(g)	(eq. mol)
B-PUA	10	1	2.32	1	–	0
UPy:15-PUA	20	1	4.18	0.85	0.68	0.15
UPy:30-PUA	32.5	1	5.26	0.70	2.22	0.30

Table 2 The composition of the UV-cured UPy-containing PUAs and hybrid nanocomposites

Formulations	PUA resins % (w/w)	MMA % (w/w)	DR1173 % (w/w)	Sol–gel % (w/w)
B	72	25	3	–
B/S10	72	25	3	10
B/S20	72	25	3	20
Upy15	72	25	3	–
UPy15/S10	72	25	3	10
UPy15/S20	72	25	3	20
UPy30	72	25	3	–
UPy30/S10	72	25	3	10
UPy30/S20	72	25	3	20



Scheme 1 Preparation of UV-curable UPy-containing PUA coatings and O–I hybrid nanocomposites

Synthesis of the silica nanoparticles

The silica nanoparticles were synthesized using the sol–gel method; 7.45 g (0.03 mol) of MAPTMS and 3.12 g (0.015 mol) of TEOS were partially hydrolyzed by 1.36 g (0.075 mol) of H_2O in 1.5 g of methanol with PTSA as a catalyst. The pH of the reaction mixture was set at 4 and stirred overnight at room temperature. The sol–gel solution was obtained and stored in the refrigerator until the preparation of the formulations.

Preparation of the UV-cured UPy-containing PUA coatings and their hybrid nanocomposite materials

The compositions of UV-curable polyurethane acrylates (PUAs) and their hybrid formulations are listed in Table 2. Additionally, a diagram that illustrates the preparation process of the UV-curable formulations is described in Scheme 1.

As a general procedure, UV-curable resin (i.e., B-PUA, UPy:15-PUA, and UPy:30-PUA) was first dissolved in $CHCl_3$ and then mixed with a suitable amount of photoinitiator (Darocur 1173) and MMA in a beaker. The formulations were stirred until homogeneous and then cast onto plexiglass panels and Teflon molds. After allowing the $CHCl_3$ to evaporate overnight at room temperature, the formulations were cured with an Osram VITALUX 300-W UV lamp for 5 min. Hybrid formulations were also prepared using the same procedure by adding 10 and 20 wt.% of sol–gel solution to the corresponding PUA formulations.

Characterization techniques

Fourier transform infrared spectroscopy (FTIR) was utilized to identify functional groups and examine the chemical structure of the synthesized compounds. FTIR spectra were all scanned between 400 and 4000 cm^{-1} using the PerkinElmer ATR FTIR spectrophotometer. This device was equipped with OmniCure UV lamp apparatus and used for the analysis of the conversion of C=C double bonds using real-time FTIR spectroscopy technique. The formulations were coated on a KBr slice and then irradiated with UV light, and the C=C peak at 1640 cm^{-1} was monitored. Each sample measurement was repeated three times.

The chemical structures of the NCO-MIC building block, U–OH oligomer, and UPy:30-PUA resin were studied using proton nuclear magnetic resonance spectroscopy (^{1}H NMR) utilizing a Varian VX 400 BB-type NMR spectrometer. The ^{1}H NMR spectra of the samples were recorded in deuterated chloroform ($CDCI_3$) using TMS as an internal standard.

The water absorptions of the UV-cured films were determined as follows: The films were cut into pieces and dried for a day in a vacuum oven to determine their dry weight (m_1). They were then immersed in distilled water at room temperature for 48 h. The swelled samples were weighed (m_2) after being dabbed with filter paper. An average of five measurements was taken for the calculation of water absorption values. The water absorption (w) values of the UV-PUA films are obtained using Eq. 1.

The chemical resistance of the coatings was evaluated by immersing them in solutions of 10% (v/v) acetic acid, NaOH, and HCI for 24 h. After that, the films were left to dry at room temperature for the night. The weight loss percentage of the films is also calculated by Eq. 1.

$$w\,(\%) = \frac{m_2 - m_1}{m_1} x100 \tag{1}$$

where m_1 is the weight of dry films and m_2 is the weight of the soaked films. The same procedure was applied for the solvent resistance of the films using methanol, toluene, and chloroform.

The gel contents of the UV-cured hybrid films were obtained using the Soxhlet technique in acetone for 6 h. The gel content ratio is calculated by Eq. 2.

$$A(\%) = \frac{w_2}{w_1} x100 \tag{2}$$

where w_1 and w_2 are weights of the samples before and after the extraction, respectively.

Dynamic mechanical analysis was conducted using a DMA Q800 (TA Company, Boston, MA, USA) operating in tensile mode. The dimensions of the sample were 50 mm × 10 mm × 1 mm. The storage modulus (E') and tanδ were measured at temperatures ranging from − 30 to 120 °C, with a heating rate of 3 °C/min under a frequency of 1 Hz and a preload of 0.1 N.

Thermogravimetric analysis of the UV-cured hybrid films was recorded by a PerkinElmer Diamond TG/DTA. The films were put in a ceramic pan and heated from 50 ° to 700 °C with a fixed heating rate of 10 °C/min under the air atmosphere.

The hydrophobicity/hydrophilicity of the UV-cured coatings was tested over the contact angle (θ) measurements using sessile drop test method. The deionized water and ethylene glycol contact angles of the films were calculated at ambient temperature utilizing a Krüss (Easy Drop DSA-2) tensiometer. The contact angle data were obtained by taking an average of five measurements at different positions on the surface of the coated plexiglass panels. The measurements of each droplet were taken from both the right and left sides.

The hardness of the coatings was determined using the BYK-Gardner pendulum hardness (König/Persoz) tester according to ASTM D4366.

The PAT Paint Adhesion Test Kit according to DIN 53151 was used to achieve crosscut test results and the assessment and classification of adhesion, based on the percentage of area removed. The scale typically ranges from 0 to 5, with zero representing exceptional adhesion and five indicating poor adhesion.

A SUPRA 35 VP, LEO scanning electron microscope (SEM) was used to study the surface morphology of the UV-cured films. Before scanning, the cured films were fractured in liquid nitrogen, and then they were covered with a thin gold layer of around 300 A°.

The UV–visible spectra of the PUA hybrid films were recorded in the range of 400–800 nm by a Shimadzu UV 6010 spectrophotometer.

The tensile properties of the UV-cured films were measured using a standard strain test on a Zwick Roell 500 N test machine with a 5-N starting force and an elongation rate of 3 mm/min. The measurements were the averages of five times.

The self-healing ability of the coatings was observed with an optical microscope (Olympus BX60) equipped with an Olympus Infinity 2 camera (5X objective). To do this, plexiglass panels were slightly cut with a razor blade to make a scratch, and the samples were observed under the microscope before and after healing treatment

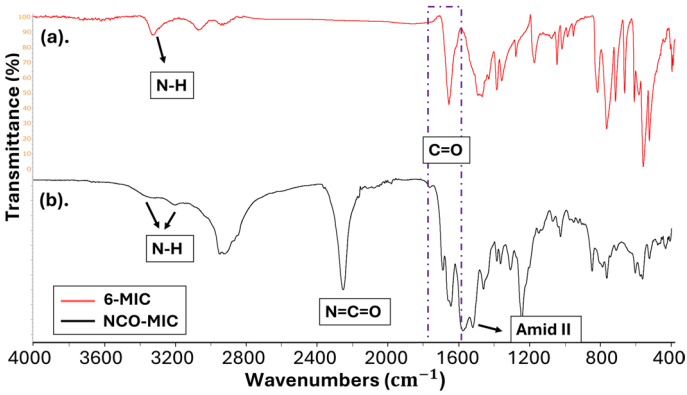


Fig. 2 The FTIR spectra of the 6-MIC (**a**) and NCO-MIC building block (**b**)

conducted at 90 °C for 10 min using a heat gun (Steinel HL 2010 E Heat Gun) from 5 cm above the plexiglass panels.

Results and discussion

Structural characterization of NCO-MIC and UV-curable PUA resins

The formation of UPy groups was monitored by the reaction between 6-MIC and IPDI with the aid of FTIR technique. The spectra of 6-MIC and NCO-MIC are shown in Fig. 2a and b, respectively. At the end of the synthesis, 6-MIC, which has amino groups, formed urea bonds upon reaction with IPDI. As the reaction proceeded, the FTIR spectrum of NCO-MIC no longer showed the stretching (str.) vibrations of the free amino groups of 6-MIC, which were determined at 3330 cm^{-1}. When N–H str. vibrations diminished, two broad absorption bands were observed

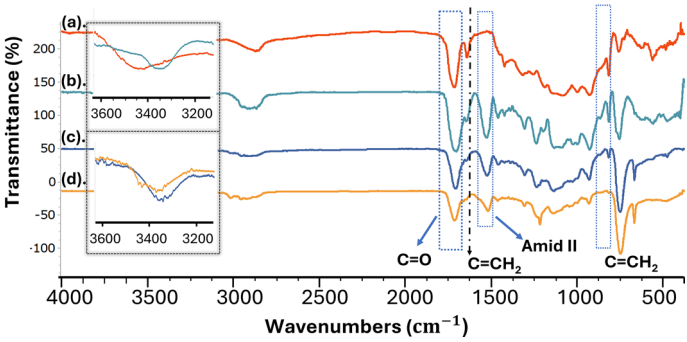


Fig. 3 The FTIR spectra of the UV-curable materials; **a** UnE-OH monomer, **b** U–OH oligomer, **c** B-PUA resin, **d** UPy:30-PUA resin

at 3200 and 3359 cm^{-1}. This change can be attributed to the –N–H str. vibrations of the urea carbonyl (–NH–(CO)–NH–). Another characteristic peak at 2256 cm^{-1} indicated the existence of the free –NCO groups. When urea groups formed, strong amid II bands were also depicted at 1577 and 1521 cm^{-1}. In both spectra, a sharp absorption band was observed at 1662 cm^{-1} in the carbonyl region, corresponding to the str. vibrations of the –C=O group of the 6-MIC. However, in the spectrum of NCO-MIC, this band was overlapped by the vibration of the –C=O group of urea at 1691 cm^{-1}. The str. vibration of the free –NCO carbonyl group of the NCO-MIC was observed at 1762 cm^{-1}.

The FTIR spectra of the unsaturated ester monomer, hydroxyl-terminated urethane oligomer, and PUA resins are shown in Fig. 3a–d. Unsaturated ester-based hydroxyl-terminated monomer (UnE-OH) was synthesized using AGE and IA. The stretching vibrations of the secondary hydroxyl group (–OH) were recorded at 3460 cm^{-1}, as shown in Fig. 3a. The strong –C=O str. vibrations of the ester group were recorded at 1718 cm^{-1}. The –C=C str. and –C–H deformation vibrations of the vinylidene groups (–C=CH_2) were observed at 1639 and 815 cm^{-1}, respectively. The structural characterization was also confirmed by the disappearance of the epoxy ring deformation vibrations at 855 and 823 cm^{-1}. When UnE-OH was reacted with an equivalent ratio of 1:1.5 of IPDI, it resulted in the formation of a hydroxyl-terminated urethane oligomer (U–OH). The FTIR spectrum of U–OH is depicted in Fig. 3b. The broad absorption band recorded at 3352 cm^{-1} belonged to the –NH str. vibrations of the urethane group, which was overlapped by the secondary –OH str. vibrations of U–OH. The –C=O str. vibrations were shifted to 1709 cm^{-1} and indicated the presence of urethane and ester carbonyl groups. The characteristic urethane group amid II band combination of –N–H deformation and –C–N str. vibrations occurred at 1529 cm^{-1}. These absorption bands and the positions proved the formation of urethane groups.

UV-curable B-PUA and UPy:30-PUA resins weresynthesized by incorporating different amounts of NCO-HEMA and NCO-MIC building blocks into the U–OH oligomer, and FTIR spectra are shown in Fig. 3c and d, respectively. The reaction continued until all –NCO groups of building blocks were consumed, as indicated by the disappearance of the characteristic –NCO peak at 2256 cm^{-1}. The –NH str. vibrations of B-PUA was recorded at 3352 cm^{-1}, and they belong to the urethane group. In the case of UPy:30-PUA, the broad –NH band was observed as two peaks at 3435 and 3352 cm^{-1}, originating from the UPy and urethane groups, respectively. B-PUA showed a broad absorption band at 1709 cm^{-1} corresponding to the str. vibrations of the urethane and ester carbonyl groups. However, this band was slightly shifted to 1716 cm^{-1} in the UPy:30-PUA spectra due to the incorporation of the carbonyl vibrations of urea. This type of shift was also determined in the amid II region. The corresponding absorption bands were recorded at 1523 and 1517 cm^{-1}, respectively. The characteristic absorption bands of the vinyl group (–C=CH_2) were observed at 1640 cm^{-1} and 816 cm^{-1}, corresponding to the –C=C str. and =C–H deformation vibrations, respectively.

The ^{1}H NMR of NCO-MIC is shown in Fig. 4. The hydrogen signals of the NCO-MIC building block are as follows: The peaks appeared at 10.0, 11.8, and 13.0 ppm that correspond to the –N–H protons of NCO–MIC, respectively. The

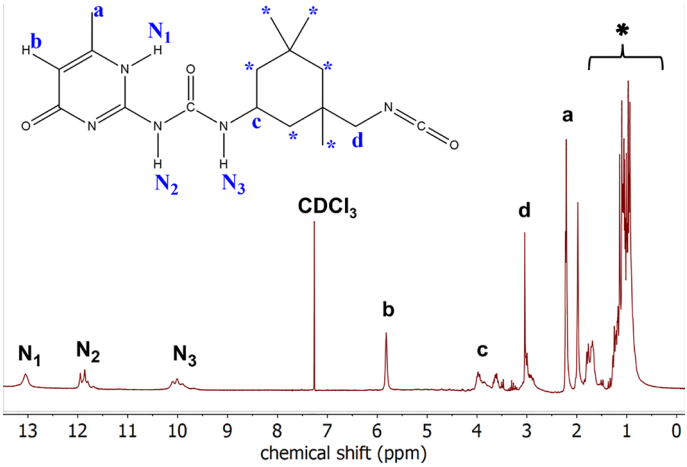


Fig.4 [1]H NMR spectrum of NCO-MIC building block (UPy moieties)

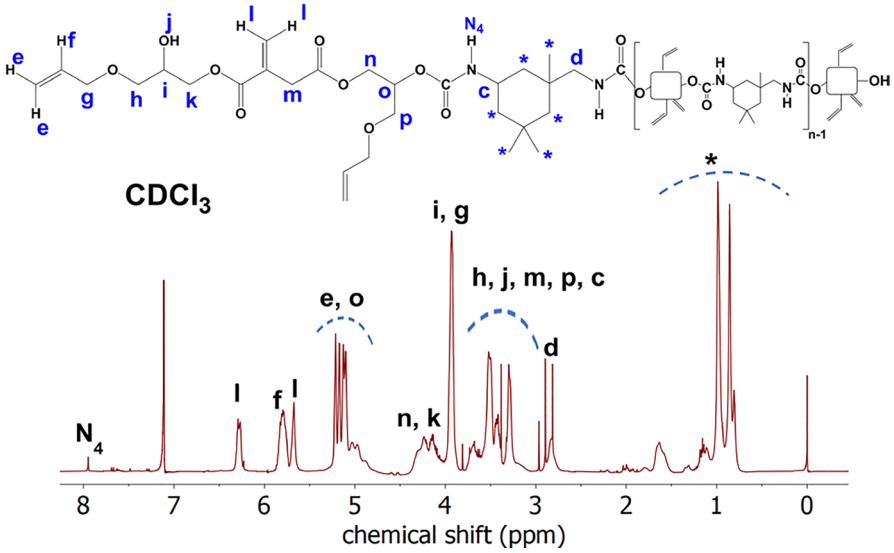


Fig. 5 [1]H NMR spectrum of U–OH oligomer

peak at 3.0 ppm belonged to the $–CH_2$ group attached to NCO moiety. This observation revealed that UPy group is attached to IPDI molecule and the reaction proceeded mainly by one –NCO group. The hydrogen signal of the pyrimidinone ring's double bond ($–C\underline{H}=C(CH_3–$) at 5.82 ppm was identified. The $–CH_2$ protons of IPDI attached to the free NCO group and the –CH proton of IPDI attached to the urea nitrogen atom are detected at 3.6 and 3.0 ppm, respectively. At 2.25 ppm, the CH_3

protons of the pyrimidinone ring were observed. The aliphatic hydrogens of isophorone moieties were detected between 1.98 and 0.95 ppm [22, 31].

The ^{1}H NMR spectrum of the U–OH oligomer in chloroform-d is given in Fig. 5. The symbolized part of the oligomer was unsaturated ester monomer (UnE-OH) which was synthesized by the reaction between the AGE and IA. Referring the Dai's research, the UnE-OH hydrogen signals of the U–OH oligomer were in good agreement with our observations [5]. In addition, the characteristic hydrogen signals of the IPDI were also identified. The H signals of the U–OH oligomer are as follows: The urethane group –NH protons were determined at 7.99 ppm. The signals at 6.28 and 5.65 ppm were assigned to the vinylidene group protons (–CH_2O(C=O)C(=C**H**$_2$)CH_2–). The methine proton of the vinyl group (CH_2=**CH**–CH_2O–) appeared at 5.8 ppm. The signals at 5.30–4.95 ppm were attributed to the methylene protons of vinyl group (**C**$\mathbf{H_2}$=$CHCH_2O$–) and methine proton of ester group (–OCH_2C**H**(CH_2OCH=CH_2)O(C=O)–), respectively. The methylene protons of ester groups are identified at 4.4–4.0 ppm. The signals between 4.0–3.15 ppm belong to the rest of the methylene and methine protons of unsaturated ester monomer. The methylene protons of IPDI attached to the urethane group are observed at 3.00–2.75 ppm. The peaks in the range of 2.00–0.5 ppm belong to methine and methylene protons of the isophorone moieties.

The chemical composition of UPy:30-PUA resin resulted in complex proton signals, as demonstrated by its ^{1}H NMR spectrum depicted in Fig. 6. The resin was synthesized through a reaction between U–OH and NCO-terminated building blocks (NCO-MIC and NCO-HEMA), with coinciding proton signals observed in Figs. 4 and 5, respectively. In addition, proton signals corresponding to the NCO-HEMA group were also identified. The UPy group signals were of low intensity due to their low content. The characteristic NH signals of the UPy group of the resin were observed at 13.04, 11.86, and 10.0 ppm, respectively, while methine and methyl

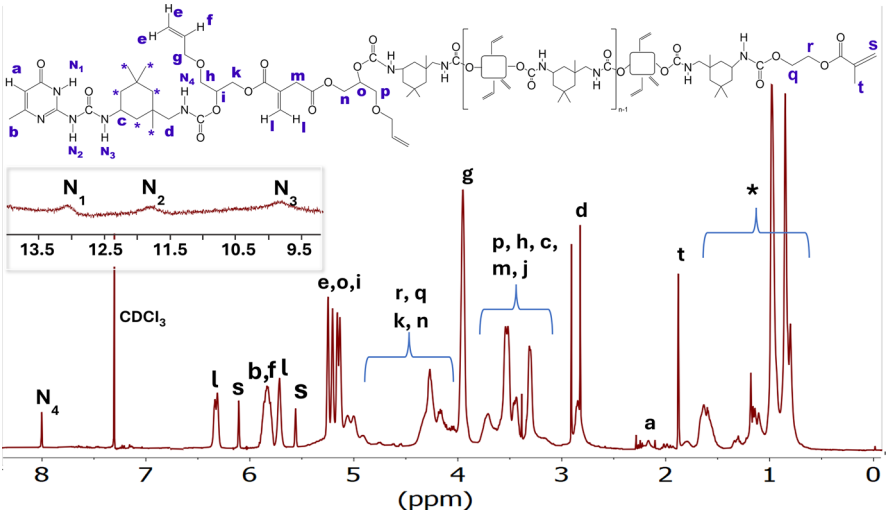


Fig. 6 ^{1}H NMR spectrum of UPy-containing PUA resin (UPy:30-PUA)

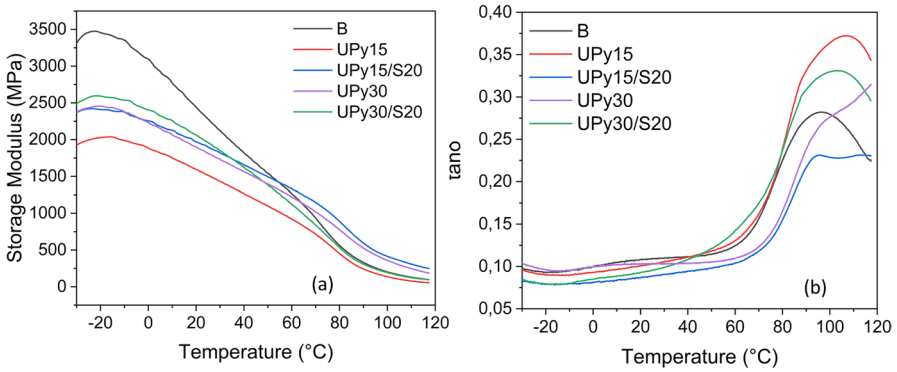


Fig. 7 DMA analysis of UPy-containing PUA coatings and hybrid nanocomposites; **a** storage modulus (E′) and **b** tanδ curves as a function of temperature

proton signals of the UPy group were detected at 5.81 and 2.22 ppm, respectively. Meanwhile, hydrogen signals of the NCO-HEMA group with higher intensity were detected as follows: The signals at 6.07 and 5.58 ppm were assigned to the = CH2 protons of the methacrylate moiety. The signals of the methyl protons adjacent to C=CH2 were recorded at 1.98 ppm, and the methylene protons were observed in the range of 4.4–4.15 ppm. The H signals of NCO-HEMA groups are in accordance with the literature [32].

Dynamic mechanical thermal analysis

Storage modulus (*E*') and tan*δ* curves of the UV-cured films as a function of temperature (°C) are given in Fig. 7a and b. As observed in the E'–T curves, the neat formulation (B) exhibited the highest storage modulus and showed a drastic change between − 30 and 120 °C when compared to UPy-containing samples. The UPy-containing samples consist of varying amounts of physically crosslinked NCO-MIC (UPy) groups and covalently crosslinked NCO-HEMA groups. The incorporation of UPy moieties into the polymer backbone leads to a decrease in the storage modulus at room temperature from 2270 to 1512 MPa and 1811 MPa, respectively, for the UPy15 and UPy30 samples, with respect to B. This decrease might be attributed to the reduction in NCO-HEMA content, which results in a lower crosslinking density of UPy-containing formulations. Thus, the UPy-containing samples exhibit higher dampness than B, indicating a greater potential for chain movement in the samples. When UPy content was increased from 15 to 30% in the polymer backbone, the storage modulus was significantly increased. This may be attributed to the increasing amount of physically crosslinking UPy groups which increased the rigidity of the sample. The incorporation of silica nanoparticles into UPy15 and UPy30 samples resulted in a considerable increase in storage modulus, reaching 1899 MPa and 1971 MPa at room temperature for UPy15/20 and UPy30/S20, respectively. This increase in storage modulus might be attributed to the increase in crosslinking density, which is a result of the Si–O–Si network. This network might impart stiffness

to the polymer matrix by creating additional covalent bonds between the silica nanoparticles and the polymer chains.

The tanδ vs. temperature curves are given in Fig. 7b. Upon heating, the tanδ values increased with the incorporation of UPy units into the polymer backbone. Furthermore, a shift in the Tg values toward higher degrees was observed. The pure sample (B) showed a Tg at 96 °C, while UPy15 and UPy30 showed Tg values of 106 °C and above 120 °C, respectively [33]. The shape and value of the tanδ curves also provide information about the change in the physical properties of the material. The narrow peaks can be associated with good polydispersity and better purity of the sample. With the addition of the UPy group and silica nanoparticles, the tanδ curves became wider when compared with the tanδ curve of neat sample (B). This increase in the width of the tanδ peak might be due to the incorporation of silica nanoparticles into the polymer matrix, which results in the presence of two different Tg dependencies, the crosslink density of polymer resin, and the Si–O–Si network. The height and area under the tanδ curves also provide essential information regarding the viscoelastic nature of the synthesized polymers. Typically, an increase in the elastic nature of the polymer matrix results in a decrease in the height of the tanδ peak. Moreover, a large area under the tanδ curve indicates a high degree of chain mobility, which translates into better damping properties and the ability to absorb and dissipate energy. When the UPy group was added to the polymer backbone, the height of tanδ peaks increased when compared to B, which meant that viscous nature of the materials was imparted. The reverse effect was observed when silica nanoparticles were introduced into the polymer matrix. The reduced value of tanδ can be attributed to the restrictions imposed by the silica nanoparticles, which limit the molecular motion of the polymer chain and result in a more elastic response of the material.

The relationship between crosslinking density (ρx) and the storage modulus can be derived from the kinetic theory of rubber elasticity and can be calculated from Eq. 3 [21].

$$\rho x = \frac{E'}{2(1+\gamma)RT} \tag{3}$$

where E' is the rubbery storage modulus, R is the gas constant (8.3145 J/mol K), T is the temperature in Kelvin, and γ is the Poisson's ratio which was estimated as 0.5. The storage modulus at the glass transition temperature was used to calculate the crosslink density of the samples, and the results are given in Table 3.

Based on the findings, it was observed that the introduction of UPy groups into the polymer backbone resulted in a significant reduction of the crosslink density from 23.8×10^3 to 9.94×10^3 mol/cm^3. This decrease can be attributed to the reduction of NCO-HEMA content, which led to the decrease in crosslink density. However, the incorporation of sol–gel nanoparticles into UPy15 resulted in an increase in crosslinking density to 31.8×10^3 mol/cm^3. This increase can be attributed to the introduction of acrylate groups of sol–gel coupling agents (MAPTMS), which led to an increase in the overall crosslink density. As the UPy content was increased in the hybrid formulations, the crosslink density was decreased to 18.36×10^3 mol/cm^3

Table 3 Thermomechanical and thermal properties of UPy-containing PUAs and hybrid nanocomposites

Samples	Tg (°C)	E'[b] (MPa)	ρx[c] ($\times 10^3$ mol/cm^3)	$T_{5\%}$[d] (°C)	$T_{50\%}$[d] (°C)	Peak maxima of 1st degradation[e] (°C)	Peak maxima of 2nd degradation[e] (°C)	Peak maxima of 3rd degradation[e] (°C)	Char yield at 700 ° C (%)
B	96	235.4	23.8	193	396	329	418	526	3.17
B/S20	–	–	–	186	410	328	422	570	7.1
UPy15	103	94.23	9.94	170	394	329	412	528	2.53
UPy15/S20	105	374.09	31.8	195	396	319	413	568	5.35
UPy30	ND	ND	ND	165	390	325	411	538	2.31
UPy30/S20	106.5	176.09	18.76	176	404	327	417	558	4.67

[a]Determined by analyzing tanδ curves using DMA analysis, [b]storage modulus of the samples at Tg from DMA analysis, [c]crosslink density of the samples according to DMA obtained by using Eq. 3, [d]determined by TGA analysis, [e]data not determined were indicated as ND

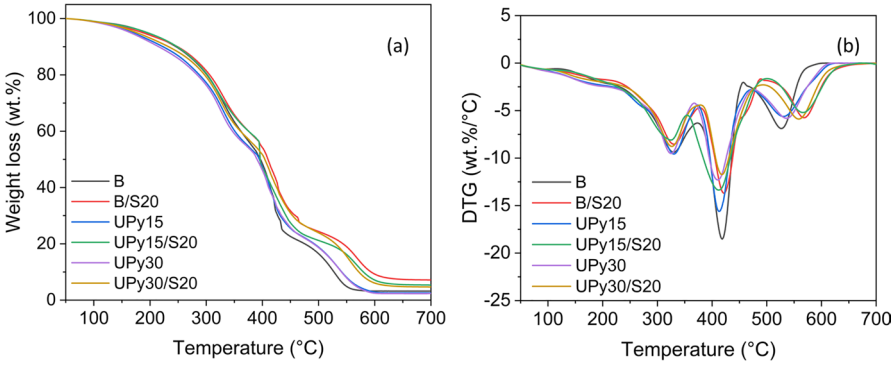


Fig. 8 TGA thermograms of the UPy-containing PUAs and hybrid nanocomposites, **a** weight loss % vs. temperature and **b** DTG vs. temperature

for UPy30/S20 despite the presence of additional physical crosslinks. Typically, a higher crosslink density leads to a higher Tg, resulting in materials with less UPy content having a higher Tg due to increased crosslinking.

Thermogravimetric Analysis

The weight loss percentage (TG; %wt) and derivative of weight loss percentage (DTG; %wt/°C) of UPy-containing PUAs and their hybrids are shown in Fig. 8. In Table 3, the peak maxima temperatures of the three main degradation phases are listed along with the temperatures at 5% weight loss ($T_{5\%}$) and 50% weight loss ($T_{50\%}$). TGA was performed under dry air. TG and DTG plots provided valuable information about thermal properties of materials. In general, the temperatures of 5% weight loss ($T_{5\%}$) and 50% weight loss ($T_{50\%}$) can be considered as indicators of the thermal stability of the materials. Moreover, DTG reveals starting and ending points of segmental lost, and the height of the peak maxima indicates the speed of segmental lost. UPy-containing PUAs and their nanocomposites exhibited three main degradation stages with similar thermograms. The weight loss smaller than 10% could be due to the oxidation of the trapped volatiles and unreacted components in the air atmosphere [34]. Among the synthesized polymers, UPy15/S20 exhibited highest $T_{5\%}$ at 195°C. On the other hand, the lowest $T_{5\%}$ was determined with UPy30 polymer at 165 °C. Besides that, B/S20 showed the highest $T_{50\%}$ at 410 °C. The lowest one belonged to the UPy30 at 390°C. The results showed that with the increasing amount of UPy content in the polymer backbone, $T_{5\%}$ and $T_{50\%}$ values were slightly decreased when compared to the neat formulation (B). This phenomenon was also observed in all degradation stages. This can be attributed to the decrease in crosslinked density, as the ratio of NCO-HEMA/NCO-MIC decreased. In addition, physically crosslinked UPy units could increase chain mobility during heating because these dynamic

H-bonds break more easily than covalent bonds and therefore decompose at lower temperatures as less energy is required, leading to a decrease in thermal decomposition temperatures [35].

The DTG curves showed three peak maxima that were in a similar temperature range for UPy-containing PUAs. Additionally, incorporation of 20% of silica nanoparticles into UPy-containing PUAs caused slight increase in thermal stability. This can be seen from the $T_{5\%}$ values of UPy15 and UPy30, which were increased from 170 to 195 °C and 165 to 176 °C, respectively. This observation can be ascribed to the high specific heat of inorganic silica nanoparticles and increasing crosslinking density of the cured films due to sol–gel precursors [28, 29]. The height of peak maxima indicates the rate of degradation in the DTG thermogram. The neat formulation showed highest degradation. When silica nanoparticles were introduced into samples, the height of peak maxima decreased, which means thermal degradation also decreased. The same effect was also observed with the increasing UPy content.

Mechanical properties

The mechanical properties of the samples were investigated by stress–strain test. Young's modulus (E), tensile strength at break (σ), and elongation at break (ε) values of the UV-cured UPy-containing films and their nanocomposites are given in Table 4. The representative stress–strain curves of the samples are also presented in Supplementary Information (Figure S1).

Chemical composition and crosslink density are significantly important on the mechanical properties of polymeric films. The results showed that with the incorporation of UPy units into the polymer backbone, tensile strength and Young's modulus of the samples were not drastically changed, but only a slight decrease was observed when compared to neat formulation (B). This can be ascribed to the decrease in NCO-HEMA content, which was led to a decrease in crosslinking density, reducing the rigidity of the cured film. When the UPy content was increased from 15 to 30%, a slight increase on tensile strength, Young's modulus,

Table 4 The mechanical properties of UPy-containing PUAs and hybrid nanocomposites

Samples	Young's modulus (E), (MPa)	Tensile strength at break (σ), (MPa)	Elongation at break (ε), (%)
B	423	12.4	4.09
B/S10	474	13.2	2.02
B/S20	502	15.4	1.81
UPy15	402	10.8	5.02
UPy15/S10	425	12.0	3.28
UPy15/S20	457	14.7	2.10
UPy30	410	11.6	5.60
UPy30/S10	390	10.2	3.22
UPy30/S20	452	11.0	2.92

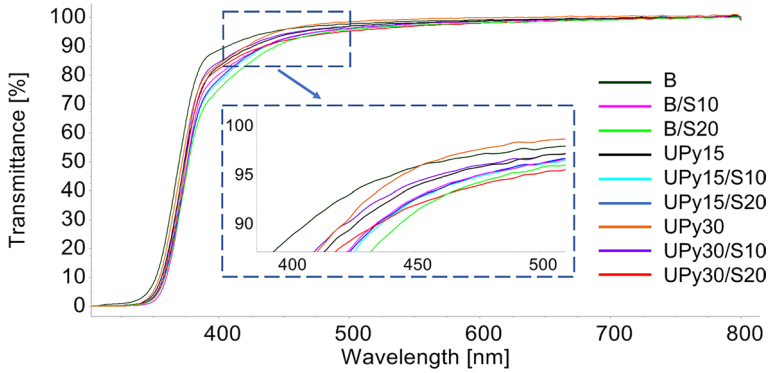


Fig. 9 Transparency of the UV-cured UPy-containing PUAs and hybrid nanocomposites

and elongation at break values were observed. These results might be ascribed to the physical crosslinking of quadruple H-bonding UPy units [23]. Slight increment on the elongation at the break values can be attributed to the physically crosslinked UPy units, which reduced the stiffness of the material. Thus, that enhanced the flexibility of cured samples. It was also observed that the nanocomposites of the UV-cured films had a tendency to increase Young's modulus and tensile strength values [16]. This can be ascribed to the increase in silica content that leads to a higher crosslink density by the formation of Si–O–Si network which led to a decrease in elongation at break values.

Transparency of the UV-cured UPy-containing PUAs and their nanocomposites

The optical transparencies of the cured films were evaluated by a UV–visible spectrophotometer. The UV–visible spectra of the cured films are shown in Fig. 9. The results showed that all UV-cured samples exhibited good transmittance above 95%

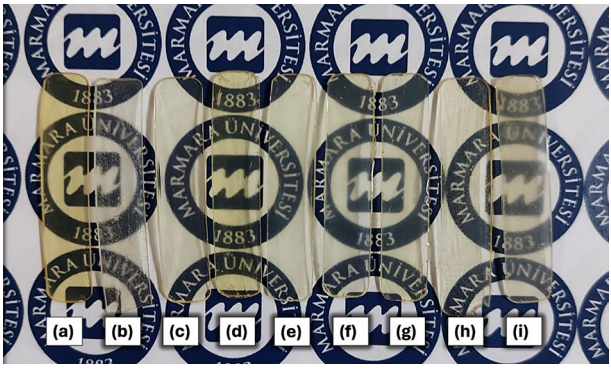


Fig. 10 The photographs of the UV-cured samples **a** B, **b** B/S10, **c** B/S20, **d** UPy15, **e** UPy15/S10, f UPy15/S20, **g** UPy30, **h** UPy30/S10, **i** UPy30/S20

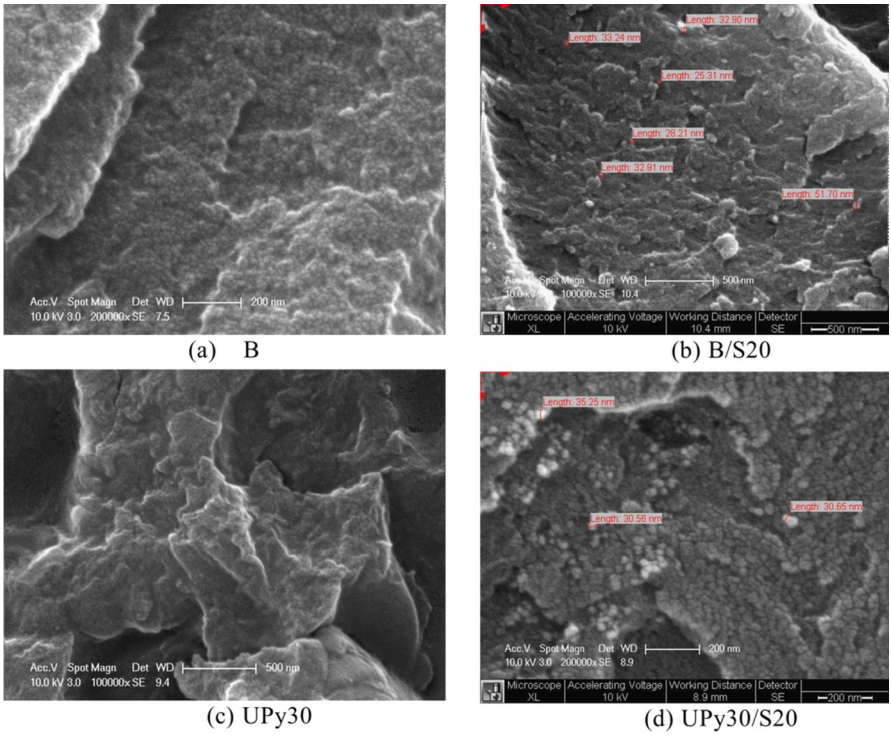


Fig. 11 The SEM images of PUAs **a** B, **b** B/S20, **c** UPy30, **d** UPy30/S20

between 500–800 nm. Additionally, UPy30 reached 95% transparency at 450 nm which was closest to the neat formulation (B) which showed the best optical transparency among other UPy-containing samples. However, UPy30/S20 showed the least optical transparency among the others. Besides, the hybrid nanocomposites tended to exhibit slightly lower transmittance values than the neat PUA formulations [37]. These results are in good agreement with the UV-cured polymeric strips as can be seen in Fig. 10.

Morphological properties

The morphological properties of the synthesized materials were analyzed by using scanning electron microscopy. The SEM images of the fractured surfaces of the PUA coatings (B, UPy30) and their hybrid nanocomposites (B/S20, UPy30/S20) are shown in Fig. 11. Upon analysis of the SEM images, it was observed that all samples were uniformly homogenous, indicating a successful incorporation of silica nanoparticles into both B and UPy30 without any phase separation. Besides, the silica nanoparticles exhibited a uniform distribution without any agglomeration in the PU matrix, despite a high loading of 20%. The average particle sizes of the hybrid films

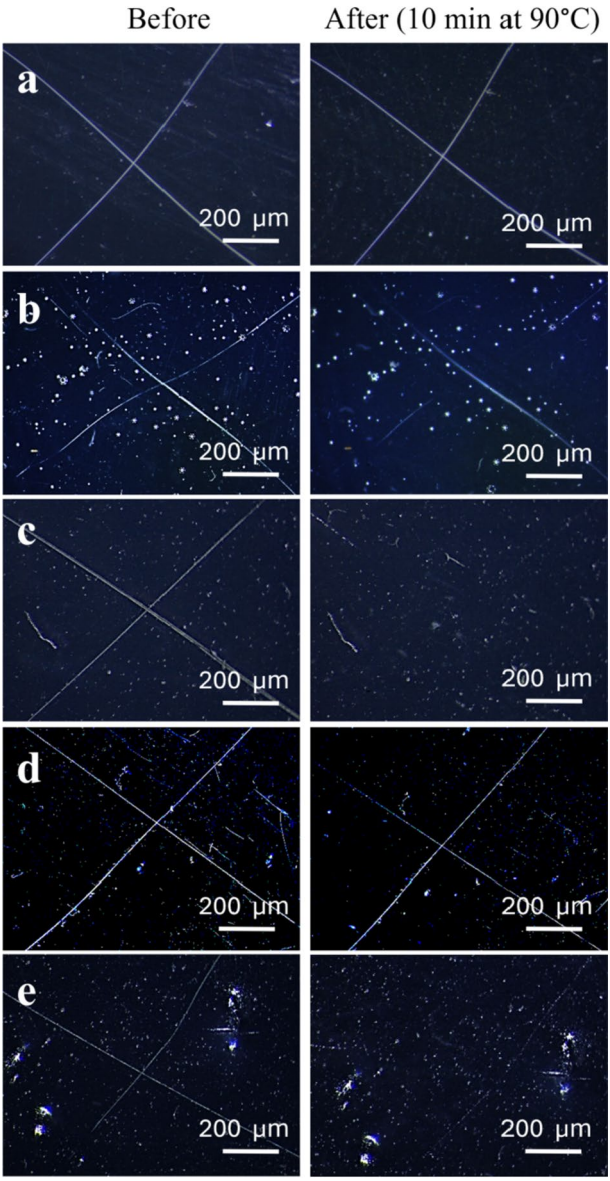


Fig. 12 Investigation of self-healing properties (images of the UV-cured specimens on plexiglass panels before and after treatment with a heat gun at 90 °C for 10 min, **a** B, **b** UPy15, **c** UPy30, **d** UPy15/S10, **e** UPy30/S10)

were measured as 31.6 and 33.5 nm for BS/20 and UPy30/S20, respectively. This result suggests the good compatibility of the silica nanoparticles with the polymer matrix. The incorporation of MAPTMS as a coupling agent in the sol–gel solution

may have played a role in this compatibility, owing to its acrylate groups that form covalent bonds with the polymer matrix upon exposure to UV light. These observations can be attributed to the strong chemical interactions between the organic and inorganic phases.

Self-healing properties

The self-healing ability of the samples was evaluated by scratching the surface of the coatings with a razor blade, and then heating them at 90 °C for 10 min using a heat gun. The observations were studied using an optical microscope, and images are given in Fig. 12. Neat formulation (B) did not show any healing ability. Among the UPy-containing samples, UPy30 showed the best self-healing ability. The scratch was entirely healed after the heat treatment, as shown in Fig. 12c. According to the estimation, heat treatment breaks the H-bonding between UPy units and consequently eliminates the crosslinked components in the sample. The scratched areas were filled at the same time with highly mobile chains. When the scratched areas were simultaneously filled with highly mobile chains and cooled to ambient temperature, the H-bonding phenomenon reappeared, leading to the observation of surface healing [13, 24]. On the other hand, only minor healing was noticed with UPy15's healing performance. This could be explained by an increase in NCO-HEMA content when compared to UPy30. This enhanced the covalent bonds in UPy15, creating a strongly crosslinked network that limits chain mobility and reduced healing ability. The hybrid coatings containing 10% of sol–gel solution (silica content) also showed slight healing ability which can be seen from Fig. 12d–e. The samples with 20% of silica did not show any healing ability. This can also be attributed to the increase in crosslinking density of the Si–O–Si network which might reduce the chain mobility of the coatings.

Table 5 Coating properties of UV-cured UPy-containing PUAs and hybrid nanocomposites

Samples	Gel content (wt%)	Water absorption (wt %)	Contact angle (θ°)		Crosscut adhesion	Pendulum hardness (König)
			Water	Ethylene glycol		
B	97.3	4.1	64	41	0	131
B/S10	98.2	3.7	74	56	0	140
B/S20	99.0	3.6	76	58	0	148
UPy15	95.8	4.9	74	59	0	127
UPy15/S10	96.7	4.5	77	62	0	135
UPy15/S20	98.0	4.2	79	62	0	142
UPy30	93.6	5.0	77	60	0	124
UPy30/S10	94.5	4.6	79	65	0	128
UPy30/S20	97.0	4.8	82	67	0	137

Coating properties

The fundamental characteristics of UV-cured UPy-containing PUAs and their hybrid coatings are listed in Table 5.

Gel content and water absorption results

The crosslinking density of the coatings can be determined by analyzing the gel content of the UV-cured samples, which is a crucial factor for the coating properties. As can be seen in Table 5, all samples had a gel content of over 95%, indicating a high crosslinking rate. However, the UPy:30-PUA-containing films deviated from this trend due to their decreasing NCO-HEMA content when compared with the other samples.

The water absorption values revealed that, when compared to PUAs, hybrid nanocomposite coatings exhibited less water absorption. This may be explained by the strong Si–O–Si network of the sol–gel solution, which increased crosslinking density of the material. The incorporation of UPy moieties slightly enhanced the coatings' water resistance, as evidenced by a reduction in the swelling ratio from 4.1 to 3.6 wt.% for the neat formulation and UPy30, respectively.

Contact angle test results

The sessile drop test method was used to assess the hydrophobicity of the surface of PUAs and hybrid coatings. The contact angle data (CAs°) of the samples with deionized water and ethylene glycol are shown in Table 5. The contact angles of deionized water and ethylene glycol on the plexiglass panels ranged from 64° to 82° and 41° to 69°, respectively. Deionized water/ethylene glycol contact angles for the coatings were 64°/41° for B, 74°/60° for UPy15, and 77°/69° for UPy30, respectively. The findings demonstrated that the water/ethylene glycol contact angles gradually increased as UPy moieties were incorporated into the PU backbone. Additionally, as the formulations' sol–gel content increased, all hybrid coatings displayed higher contact angle values compared to its neat PUA formulations. This might be corresponded to the formation of Si–O–Si network. Because these bonds have substantially lower surface energy than neat PUAs, these groups would migrate across the film surface during the UV-curing process, resulting in an increase in contact angles [36]. The water absorption values of the coated films also support these findings.

Pendulum hardness and crosscut test results

The pendulum hardness test is a method to measure the surface hardness of a material by analyzing the loss of kinetic energy of an oscillating pendulum in accordance with standards. The time taken for the pendulum to oscillate is inversely proportional to the surface hardness of the material. The pendulum hardness of the UV-cured PUA coatings increased in the following order:

B/S20 > UPy15/S20 > B/S10 > UPy30/S20 > UPy15/S10 > B > UPy30/S10 > UPy15 > UPy30. Differences in crosslinking density could be the driving force of this type of trend. Higher double bonds of the material in UV-cured coatings result in higher crosslinking densities, which determine the hardness. The pendulum hardness of PUA coatings decreased with an increase in UPy content in the backbone. This is because the NCO-HEMA content, which provides the PUA backbone's double bond composition, was reduced. The results also showed that hybrid nanocomposite coatings were found to have higher hardness than PUA coatings. This might be due to the strong Si–O–Si network formation of the hybrid nanocomposite coatings and good compatibility between the silica nanoparticles and PUA polymer matrix. In addition, all the PUAs and their hybrid nanocomposite coatings showed excellent adhesion to the plexiglass panels according to crosscut test results.

Chemical and solvent resistance

During the testing phase, acetic acid (AcH), sodium hydroxide (NaOH), and hydrochloric acid (HCI) at 10% weight each were used to assess the chemical resistance of the UV-cured samples, while toluene, methanol, and chloroform were used to test their solvent resistance. All the samples were soaked in the respective chemicals and solvents for one day before being dried at room temperature. The weight loss percentages of the samples are listed in Table 6.

According to results, all samples showed good resistance to chemicals, and there were no changes in their physical appearance. In comparison with the neat PUAs, the hybrid nanocomposites demonstrated superior solvent and chemical resistance. When the samples were treated with the solvents, all of them showed a slight yellowing effect with toluene and $CHCI_3$. The neat formulation (B) showed the highest

Table 6 Solvent and chemical resistance of the UV-cured coating materials

Samples	Solvent resistance (Weight loss, wt %)			Chemical resistance (Weight loss, wt%)		
	Toluene	Methanol	$CHCI_3$	AcH (10%)	NaOH (10%)	HCI (10%)
B	0.9	7.5	4.3	1.8	3.1	1.7
B/S10	0.7	6.9	2.7	0.7	2.5	1.3
B/S20	0.7	5.8	2.5	0.3	2.1	1.2
UPy15	2.1	6.7	5.0	2.4	4.2	2.0
UPy15/S10	1.5	6.6	4.7	1.8	2.7	1.4
UPy15/S20	0.6	6.2	2.2	1.2	2.5	1.2
UPy30	2.4	8.9	7.4	1.9	4.4	1.9
UPy30/S10	1.4	8.0	7.3	1.0	3.2	1.4
UPy30/S20	2.2	6.9	4.0	0.9	2.7	2.1

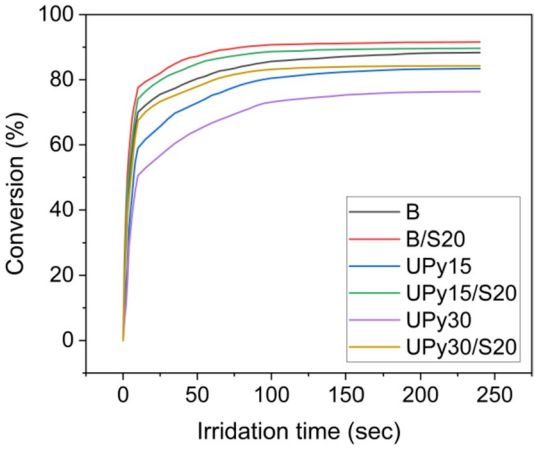


Fig. 13 Double bond conversions of the UV-curable formulations

yellowing among other samples. However, the yellowing effect decreased with an increase in the amount of UPy content, as well as with the increase in the silica content. It is noteworthy that UPy:30-PUA-containing samples displayed a slight reduction in transparency upon methanol treatment, indicating the influence of UPy content on the coating's chemical resistance.

Double bond conversion of the UV-cured films

The UV-curing process of the samples has been investigated using real-time FTIR spectroscopy, by monitoring the C=C–H out-of-plane bending vibration at 816 cm^{-1} during the crosslinking process. The results have been calculated as percentages using Eq. 4,

where P represents the absorption peak area, t is any given time, and 0 is the absorption peak area before

$$\text{degree of conversion} = \frac{[(P)816]0 - [(P)816]t}{[(P)816]0} x100 \quad (4)$$

UV irradiation [15]. The results are presented in Fig. 13.

The double bond conversion degree of the tested samples ranged between 91.6 and 76%, with the following order: B/S20 > UPy15/S20 > B > UPy30/S20 > UPy15 > UPy30. The hybrid nanocomposites displayed higher and faster conversion rates in comparison with UV-cured PUA coatings. This can be attributed to the presence of MAPTMS, a coupling agent in the sol–gel formulation which contributes to the double bond content. Additionally, the results indicated good compatibility between the polymer matrix and the silica nanoparticles. As the amount of UPy content was increased, the samples exhibited a decrease in C=C bond conversions. This decrease in conversion can be attributed to the reduction in double bond content resulting from the decrease in NCO-HEMA ratio in the PUA resin.

Conclusion

In this study, UV coating materials with quadruple H-bonding UPy groups were obtained to achieve thermally triggered scratch healing ability without compromising their mechanical and thermal properties. Their hybrid nanocomposites were also prepared by mixing 10 and 20 wt% sol–gel solution into the UPy-containing PUA formulations. The results suggest that the thermomechanical properties of the samples improved with an increase in UPy content, as indicated by the shifting of *T*g values toward higher degrees. Incorporating UPy moieties did not have any significant impact on the thermal decomposition and mechanical properties, even with a decrease in crosslinking density due to the decrease in NCO-HEMA content. Moreover, hybrid nanocomposites showed better thermal and mechanical properties than the neat PUA formulations. The SEM analysis revealed that the distribution of silica nanoparticles was homogeneous, which is consistent with the enhancement of thermal and mechanical properties of the hybrid nanocomposites. The formulation with the highest UPy content (UPy30) also demonstrated good scratch healing when thermally treated at 90 °C for 10 min. Furthermore, all the samples exhibited good adhesion to the plexiglass panels and resistance to solvents and chemicals. The transmittance of the samples was above 95% in most of the visible region, indicating good optical transparency. Overall, our results demonstrate the potential of the UPy-containing coatings and hybrid nanocomposites for coating industry.

Supplementary Information The online version contains supplementary material available at https://doi.org/10.1007/s00289-024-05226-9.

Acknowledgments This study was supported by Marmara University Science Fund (FEN-C-YLP-130219-0040), and the author M. Çınar acknowledges Council of Higher Education of Türkiye (CoHE) for the 100/2000 Doctoral scholarship (TB-121-01.08.03).

Author contributions Mert Çınar was involved in formal analysis, investigation, conceptualization, project administration, writing—original draft, writing—review and editing, and visualization. Sevim Karataş participated in conceptualization, methodology, supervision, resources, writing—review and editing, and visualization. Gökhan Çaylı helped with formal analysis, writing—review and editing, and visualization.

Funding Open access funding provided by the Scientific and Technological Research Council of Türkiye (TÜBİTAK). This study was funded by Marmara University Science Fund, FEN-C-YLP-130219-0040, and the author M.Çınar was funded by Council of Higher Education of Türkiye (CoHE 100/2000 Doctoral Scholarship), TB-121-01.08.03.

Declarations

Conflict of interest The authors declare no competing interests.

Open Access This article is licensed under a Creative Commons Attribution 4.0 International License, which permits use, sharing, adaptation, distribution and reproduction in any medium or format, as long as you give appropriate credit to the original author(s) and the source, provide a link to the Creative Commons licence, and indicate if changes were made. The images or other third party material in this article are included in the article's Creative Commons licence, unless indicated otherwise in a credit line to the material. If material is not included in the article's Creative Commons licence and your intended use is not permitted by statutory regulation or exceeds the permitted use, you will need to obtain permission

directly from the copyright holder. To view a copy of this licence, visit http://creativecommons.org/licenses/by/4.0/.

References

1. Zhang Y, Rocco C, Karasu F, van der Ven LGJ, van Benthem RATM, Allonas X, Croutxé-Barghorn C, Esteves ACC, de With G (2015) UV-cured self-replenishing hydrophobic polymer films. Polymer 69:384–393. https://doi.org/10.1016/j.polymer.2015.02.036
2. Kaewpirom S, Kunwong D (2012) Curing behavior and cured film performance of easy-to-clean UV-curable coatings based on hybrid urethane acrylate oligomers. J Polym Res. https://doi.org/10.1007/s10965-012-9995-1
3. Dupont EP, Luisier R, Gijs MAM (2010) NOA 63 as a UV-curable material for fabrication of microfluidic channels with native hydrophilicity. Microelectron Eng 87:1253–1255. https://doi.org/10.1016/j.mee.2009.11.084
4. Jiao X, Song Y, He N, Wang X, Huang M, Zhang L, Li X, Xu J, Chen J, Li W, Lai G, Hua X, Yang X (2022) High tensile strength UV-cured castor oil-based silicone-modified polyurethane acrylates. ACS Omega 7:12680–12689. https://doi.org/10.1021/acsomega.1c06959
5. Dai J, Liu X, Ma S, Wang J, Shen X, You S, Zhu J (2016) Soybean oil-based UV-curable coatings strengthened by crosslink agent derived from itaconic acid together with 2-hydroxyethyl methacrylate phosphate. Prog Org Coat 97:210–215. https://doi.org/10.1016/j.porgcoat.2016.04.014
6. Liu F, Liu G (2018) Enhancement of UV-aging resistance of UV-curable polyurethane acrylate coatings via incorporation of hindered amine light stabilizers-functionalized TiO_2-SiO_2 nanoparticles. J Polym Res. https://doi.org/10.1007/s10965-018-1466-x
7. Sangermano M, Foix D, Kortaberria G, Messori M (2013) Multifunctional antistatic and scratch resistant UV-cured acrylic coatings. Prog Org Coat 76:1191–1196. https://doi.org/10.1016/j.porgcoat.2013.03.030
8. Hong JW, Cheon HK, Kim SH, Hwang KH, Kim HK (2017) Synthesis and characterization of UV curable urethane acrylate oligomers containing ammonium salts for anti-fog coatings. Prog Org Coat 110:122–127. https://doi.org/10.1016/j.porgcoat.2017.03.009
9. Folmer BJB, Sijbesma RP, Versteegen RM, van der Rijt JAJ, Meijer EW (2000) Supramolecular polymer materials: chain extension of telechelic polymers using a reactive hydrogen-bonding synthon. Adv Mater 12:874–878. https://doi.org/10.1002/1521-4095(200006)12:12%3C874::AID-ADMA874%3E3.0.CO;2-C
10. Nojiri S, Yamada H, Kimata S, Ikeda K, Senda T, Bosman AW (2016) Supramolecular polypropylene with self-complementary hydrogen bonding system. Polymer 87:308–315. https://doi.org/10.1016/j.polymer.2016.02.010
11. Sivakova S, Rowan SJ (2005) Nucleobases as supramolecular motifs. Chem Soc Rev 34:9–21. https://doi.org/10.1039/b304608g
12. Cheng S, Zhang M, Dixit N, Moore RB, Long TE (2012) Nucleobase self-assembly in supramolecular adhesives. Macromolecules 45(2):805–812. https://doi.org/10.1021/ma202122r
13. Beijer FH, Sijbesma RP, Huub Kooijman AL, Spek EWM (1998) Strong dimerization of ureidopyrimidinones via quadruple hydrogen bonding. J Am Chem Soc 120:6761–6769. https://doi.org/10.1021/ja974112a
14. Hu JL, Mo R, Jiang X, Sheng X, Zhang X (2019) Towards mechanical robust yet self-healing polyurethane elastomers via combination of dynamic main chain and dangling quadruple hydrogen bonds. Polymer 183:121912–121912. https://doi.org/10.1016/j.polymer.2019.121912
15. Liu R, Yang X, Yuan Y, Liu J, Liu X (2016) Synthesis and properties of UV-curable self-healing oligomer. Prog Org Coat 101:122–129. https://doi.org/10.1016/j.porgcoat.2016.08.006
16. Neikirk C, Chung J, Priestley RD (2015) Modification of mechanical properties in polymer nanocomposites by the incorporation of specific self-complementary hydrogen bonding interactions. Polymer 79:212–220. https://doi.org/10.1016/j.polymer.2015.10.019
17. Zhang Z, Cheng L, Zhao J, Zhang H, Zhao X, Liu Y, Bai R, Pan H, Yan X (2020) Muscle-mimetic synergistic covalent and supramolecular polymers: phototriggered formation leads to mechanical performance boost. J Am Chem Soc 143:902–911. https://doi.org/10.1021/jacs.0c10918

18. Yan X, Liu Z, Zhang L, Lopez J, Wang H, Wu H-C, Niu S, Yan H, Wang S, Lei T, Li J, Qi D, Huang P, Huang J, Zhang Y, Wang Y, Li G, Tok J-H, Chen X, Bao Z (2018) Quadruple H-bonding cross-linked supramolecular polymeric materials as substrates for stretchable antitearing, and self-healable thin film electrodes. J Am Chem Soc 140:5280–5289. https://doi.org/10.1021/jacs.8b01682
19. Wang X, Li Y, Qian Y, Qi H, Li J, Sun J (2018) Mechanically robust atomic oxygen-resistant coatings capable of autonomously healing damage in low earth orbit space environment. Adv Mater 30:1803854. https://doi.org/10.1002/adma.201803854
20. Song Q, Chen H, Yu W, Ni H, Hu P, Zhao K (2019) Multi-stimuli responsive polyurethane based on quadruple hydrogen bonding interactions. Mater Today Proc 16:1405–1409. https://doi.org/10.1016/j.matpr.2019.05.315
21. Manning KB, Wyatt N, Hughes L, Cook A, Giron NH, Martinez E, Campbell CG, Celina MC (2018) Self assembly-assisted additive manufacturing: direct ink write 3d printing of epoxy-amine thermosets. Macromol Mater Eng 304:1800511. https://doi.org/10.1002/mame.201800511
22. Lin F, Wang R, Liu L, Li B, Ouyang L, Liu WJ (2017) Enhanced intermolecular forces in supramolecular polymer nanocomposites. Exp Polym Lett 11:690–703. https://doi.org/10.3144/expresspolymlett.2017.67
23. Invernizzi M, Turri S, Levi M, Suriano R (2018) 4D printed thermally activated self-healing and shape memory polycaprolactone-based polymers. Eur Polymer J 101:169–176. https://doi.org/10.1016/j.eurpolymj.2018.02.023
24. Gao F, Cao J, Wang Q, Liu R, Zhang S, Liu J, Liu X (2017) Properties of UV-cured self-healing coatings prepared with PCDL-based polyurethane containing multiple H-bonds. Prog Org Coat 113:160–167. https://doi.org/10.1016/j.porgcoat.2017.09.011
25. Takahashi M, Figus C, Kichob T, Enzo S, Casula M, Valentini M, Innocenzi P (2009) Self-Organized Nanocrystalline Organosilicates in Organic-Inorganic Hybrid Films. Adv Mater 21(17):1732–1736. https://doi.org/10.1002/adma.200802937
26. Fu J, Yu H, Wang L, Liang R, Zhang C, Jin M (2021) Preparation and properties of UV-curable polyurethane acrylate / SiO2 composite hard coatings. Prog Org Coat 153:106121. https://doi.org/10.1016/j.porgcoat.2020.106121
27. Mohseni M, Bastani S, Jannesari A (2014) Influence of silane structure on curing behavior and surface properties of sol–gel based UV-curable organic–inorganic hybrid coatings. Prog Org Coat 77:1191–1199. https://doi.org/10.1016/j.porgcoat.2014.04.008
28. Wu L, Baghdachi J (2015) Functional polymer coatings: principles, methods and applications, 1st edn. Wiley, Hoboken, New Jersey
29. Corcione CE, Striani R, Frigione M (2014) Organic–inorganic UV-cured methacrylic-based hybrids as protective coatings for different substrates. Prog Org Coat 77:1117–1125. https://doi.org/10.1016/j.porgcoat.2014.03.010
30. Zheng S, Li J (2010) Inorganic–organic sol gel hybrid coatings for corrosion protection of metals. J Sol–Gel Sci Technol 54:174–187. https://doi.org/10.1007/s10971-010-2173-1
31. Janssen HM, Gemert van GML, Meijer EW, Bosman AW (2014) Preparation of supramolecular polymers containing quadruple hydrogen bonding units in the polymer backbone. (Patent No. EP 1 687 378 B1).
32. Xu R-C, Yu F, Huang L, Zhou W, Wang Y, Wang F, Sun X, Chang G, Fang M, Zhang L, Li F (2019) Isocyanate-terminated urethane-based dental adhesive bridges dentinal matrix collagen with adhesive resin. Acta Biomater 83:140–152. https://doi.org/10.1016/j.actbio.2018.11.007
33. Wietor J-L, Dimopoulos A, Govaert LE, van Benthem RATM, de With G, Sijbesma RP (2009) Preemptive healing through supramolecular cross-links. Macromolecules 42:6640–6646. https://doi.org/10.1021/ma901174r
34. Chattopadhyay DK, Webster DC (2009) Thermal stability and flame retardancy of polyurethanes. Prog Polym Sci 34:1068–1133. https://doi.org/10.1016/j.progpolymsci.2009.06.002
35. N HM, Saidi NM, Omar FS, Ramesh K, Ramesh S, Bashir S (2018) Thermogravimetric analysis of polymers, in: Encyclopedia of polymer science and technology, John Wiley & Sons Ltd, pp 1–29. https://doi.org/10.1002/0471440264.pst667
36. Çınar M, Karataş S (2022) Synthesis of polyurethane acrylate hybrids containing fluorine and siloxane by the sol–gel method for UV-curable coatings. Polym Bul. https://doi.org/10.1007/s00289-022-04619-y

37. Zhang Y, Sheng Y, Wang V, Lu X (2022) UV-curable self-healing, high hardness and transparent polyurethane acrylate coating based on dynamic bonds and modified nano-silica. Prog Org Coat 172:107051–107051. https://doi.org/10.1016/j.porgcoat.2022.107051

Publisher's Note Springer Nature remains neutral with regard to jurisdictional claims in published maps and institutional affiliations.

Authors and Affiliations

Mert Çınar[1] · Gökhan Çaylı[2] · Sevim Karataş[1]

✉ Sevim Karataş
skaratas@marmara.edu.tr

[1] Department of Chemistry, Faculty of Science, Marmara University, Göztepe, 34722, Kadıköy, Istanbul, Turkey

[2] Engineering Sciences Department, Istanbul University-Cerrahpaşa, 34320 Avcılar, Istanbul, Turkey